Science Advances

AAAS

advances.sciencemag.org/cgi/content/full/2/1/e1501168/DC1

Supplementary Materials for

Hybrid bilayer plasmonic metasurface efficiently manipulates visible light

Fei Qin, Lu Ding, Lei Zhang, Francesco Monticone, Chan Choy Chum, Jie Deng, Shengtao Mei, Ying Li, Jinghua Teng, Minghui Hong, Shuang Zhang, Andrea Alù, Cheng-Wei Qiu

Published 1 January 2016, *Sci. Adv.* **2**, e1501168 (2016)
DOI: 10.1126/sciadv.1501168

The PDF file includes:

Deviation between experiment and simulation

As we discussed in the main text, the conversion efficiency reduced to 17% in experiment from the simulation results 29%, so does the extinction ratio. The simulation results shows that the peak value of extinction ratio can reach to 12.7dB if the fabrication and characterization are in ideal conditions. The deviation of extinction ratio between the experiment and simulation may be attributed to many factors during the fabrication and characterization. For example, the presence of a cladding layer or adhesive gold grains on the sidewall of HSQ pillar is inevitable when we deposit the Au film after EBL patterning. Moreover, the thickness of the deposited gold film may not be exactly the same as the design value of 30nm. We numerically analysed the effect of these non-idealities, and our results indicate that when a cladding layer with thickness varying from 0 to 5nm is added onto the HSQ sidewall, the peak value of extinction ratio will be decreased from 12.7dB(x18.6) to 5.4dB(x3.47). In parallel, if we change the deposited gold thickness from 30nm to 20nm while all the other parameters are kept constant, the peak value of the extinction ratio will decrease from 12.7dB(x18.6) to 6.4dB(x4.37) (see Figs. S2 & S3). From these results, it can be seen that the extinction ratio is sensitive to nanofabrication details. Besides these two factors, there are still many other elements affecting the ER value, such as (i) non-uniform parameters over the entire pattern; (ii) differences in the actual material properties of gold and HSQ compared to the simulation values; (iii) the sloping HSQ pillar profile, which makes the top layer nano-antennas not exactly conformal with its Babinet complementary on the bottom; (iv) non-ideal characterization process, such as a non-ideally planar wavefront and off-normal illumination; lack of collection of higher-order diffraction signals, etc. The deviation of the extinction ratio between simulation results and experiments is the end product of all these factors.

Effect of higher-order diffraction mode

As demonstrated in the previous works, the reflection and refraction property of the metasurface follow the generalized Snell's law

$$n_t \sin\theta_t - n_i \sin\theta_i = \frac{\lambda}{2\pi}\frac{d\phi}{dx}$$

since the E_y incidence light is illuminated at normal direction from substrate side in our case, the generalized Snell's law can be written as

$$\sin\theta = \lambda/\Gamma_x,$$

where θ and Γ_x denote the deflection angle of cross-polarized component E_x and the supercell periodicities in X direction, λ is the working wavelength. For the higher diffraction order modes, the modified grating equation with abrupt phase delay can be expressed as:

$$\sin\theta_m = \frac{(m+1)\lambda}{\Gamma_x}$$

$0.5 < \frac{\lambda}{\Gamma_x} < 1$ in our design, so there should be three diffraction orders exist: the anomalous refraction order (m+1)=1, normal direction (m+1)=0, and the opposite anomalous refraction direction (m+1)= -1. The diffraction intensity of each order for the cross polarized component E_x, obtain from the numerical simulations, is shown in Fig. S4. We can see clearly from this figure that the diffraction to the 1 and -1 order have the efficiency 24.5% and 4.5% at wavelength 770 nm where has peak conversion efficiency value, and the 0 order do not has obviously refraction for the cross polarized components. As shown in Fig. 2B, however, the wavefront indeed has a small degree of non-uniformity, which should be attributed to the natural property of metasurface structure. Since the supercell of the meta-surface consists of 6 discrete nano-antennas with interfacial phase gradients and the wavefront is formed by the scattered light from these antennas, it is not possible to have the uniformity of the wavefront as good as the "ideal" plane wave. The higher order refraction components will affect the experimentally measured conversion efficiency and extinction ratio a little, but will not seriously affect the wavefront since the ratio between the major order with the order of interest is larger than 5:1.

Dependence of resonant wavelength on geometric parameters

The coupling effect plays an important role in our design, which is significantly different from previous single-layer metasurface designs. Although the dependence of resonant wavelength on geometry becomes more complex, we still can control the working wavelength by varying the width and length of each V-shaped arms. As shown in Fig. S7, while the width of nanoantennas increases from 40 nm to 65 nm with other parameters fixed the same values as those used in Fig. 3A, the resonance peaks can be blue shifted from 850 nm to 730 nm. As known, the cross polarized components of the V-shaped nanoantenna result from the summing contributions of the symmetric and anti-symmetric eigenmodes, which are excited by the components of incidence electric field polarized parallel and perpendicular to the symmetry axis of the V-shaped antennas. When the width increases, the asymmetric property of the V-shaped antennas will be weakened, so that the cross polarized components of scattered light will be decreased, that is the reason for the conversion efficiency decreased from 30% to 17% while the width is changed from 40 nm to 65 nm. In addition, as shown in Fig. S8, the working wavelength can be readily controlled from 720 nm to 800 nm by varying the length of subunit 1-3 nanoantennas from L = 110 nm, 105 nm and 100 nm to L = 140 nm, 135 nm and 130 nm. Due to the same principle, the conversion efficiency also increases from 7% to 34%. Combining with the periodicity variation and using other metals (e.g. Ag, Al, etc.), the working wavelength can be further tuned to violet or near-infrared light.

A characteristic feature of our bilayer metasurface is the presence of an HSQ pillar between the top and bottom layers, which provides an additional degree of freedom to design and control the structure. High refractive index of HSQ contributes to enhance the coupling effect between top and bottom layers. The influence of the HSQ pillar height on the conversion efficiency is also investigated. As shown in Fig. S10, by fixing other parameters, as the height of HSQ pillars increase from 30 nm to 200 nm, the highest conversion efficiency 29% is achieved when H = 100 nm. This indicates that there is an optimal thickness value of the HSQ pillar for obtaining the best coupling effect between top nanoantennas and their complementary Babinet-inverted apertures on the bottom layer. The peak position also undergoes slight shifts when the HSQ height is altered.

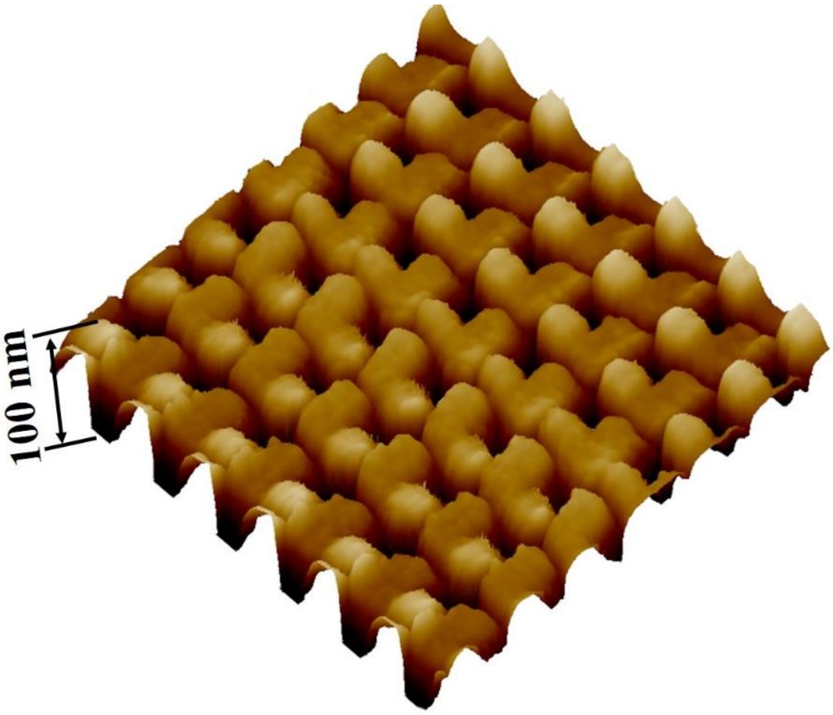

Fig. S1 Surface profile measured by AFM

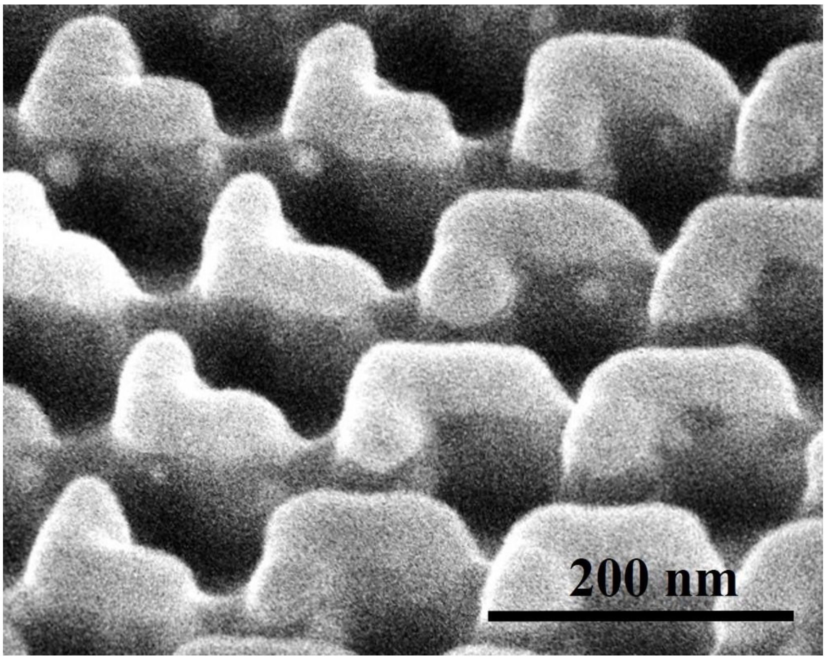

Fig. S2 Tilted SEM image of the fabricated bilayer metasurface, showing nonuniform grains of gold at the sidewall of HSQ pillars.

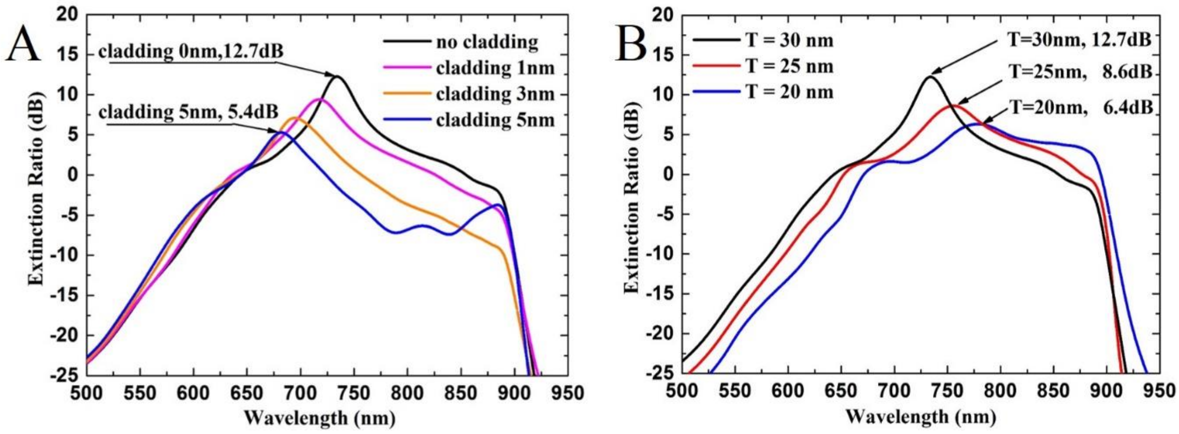

Fig. S3 Dependence of the extinction ratio on the thickness of cladding layer (A) and the thickness of deposited gold film (B)

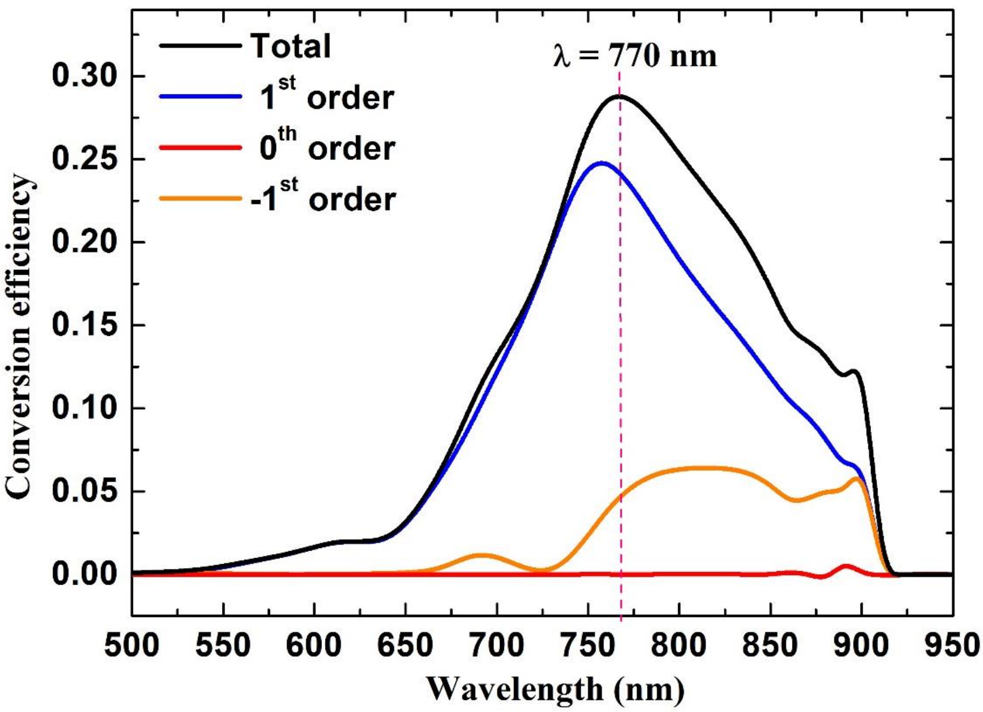

Fig. S4 Refraction efficiency of the cross-polarized component in each diffraction orders.

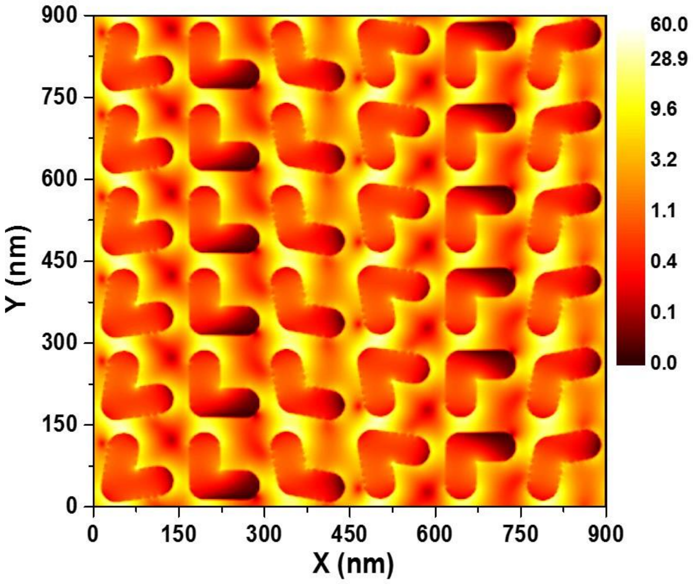

Fig. S5 Electric field distribution on the top layer of the bilayer metasurface at 770 nm (the colour map is plotted in logarithmic scale)

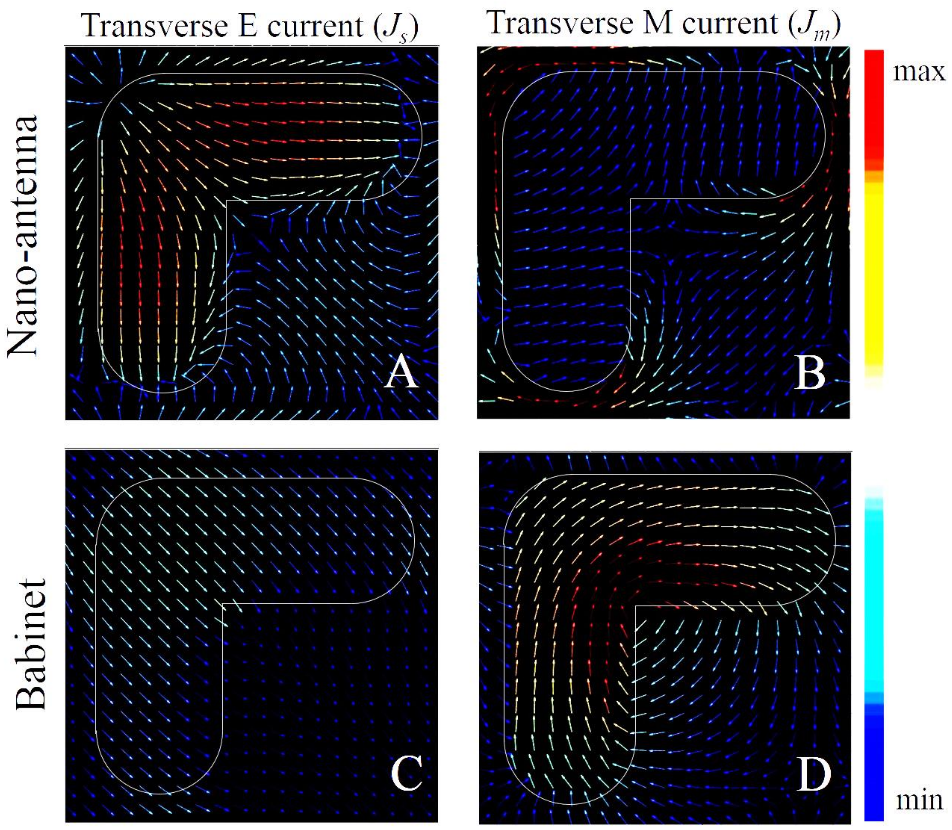

Fig. S6 Transverse electrical current (J_s) (A and C) and equivalent transverse magnetic current (J_m) (B and D) of the bilayer metasurface for the subunit 2 under symmetric excitation. The position of the V-shaped nanoantenna on the top and the Babinet-inverted aperture on the bottom are indicated by the white outlines. The amplitudes are represented by the color of the arrows, with the same relative scale for J_s and J_m, respectively.

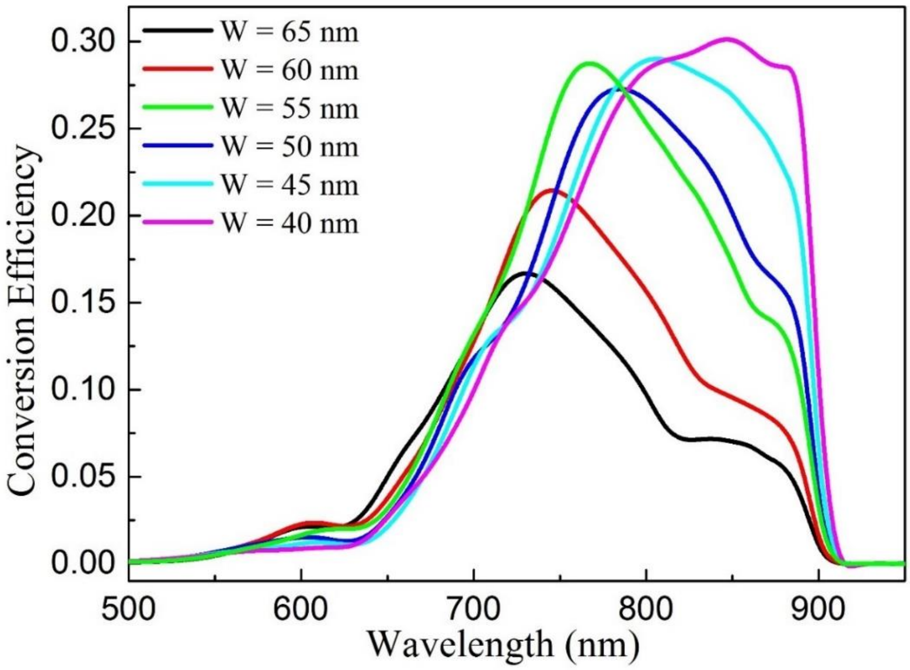

Fig. S7 Dependence of the conversion efficiency on the width of nanoantennas.

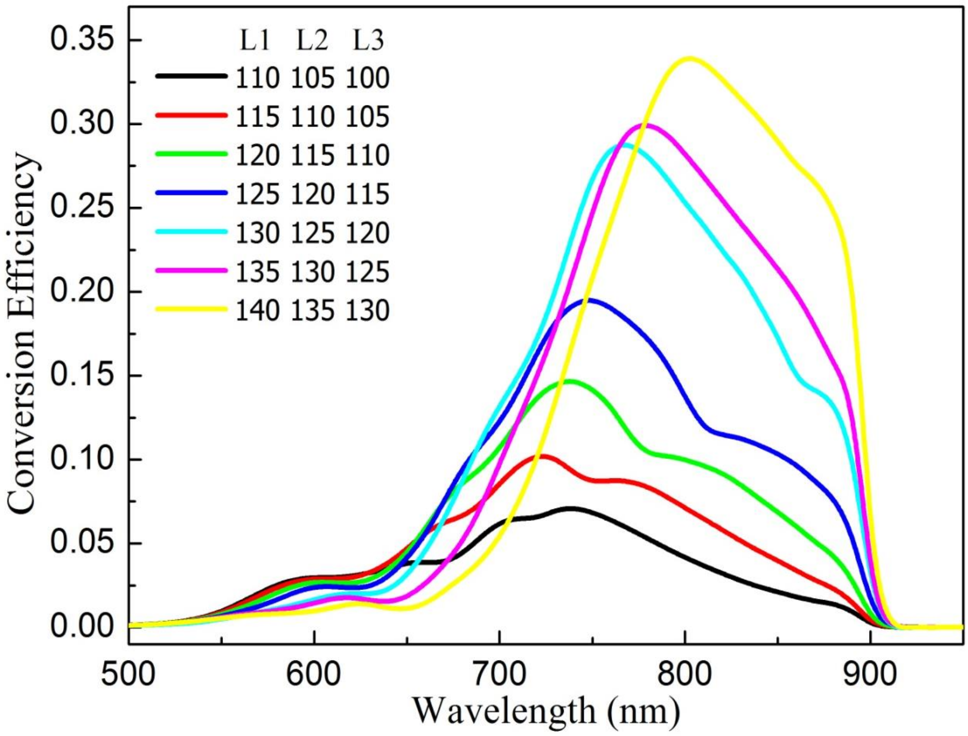

Fig. S8 Dependence of the conversion efficiency on the length of nanoantennas.

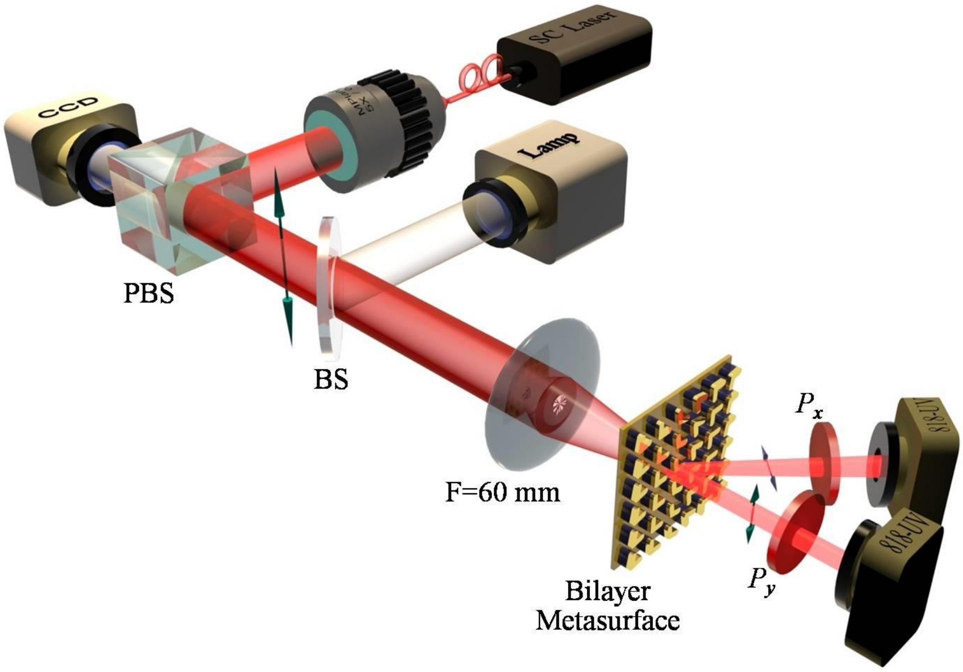

Fig. S9 Schematic representation of the optical measurement setup. PBS: polarized beam splitter; BS: beam splitter; P_x: Linear polarizer of Ex component; P_y: Linear polarizer of Ey component.

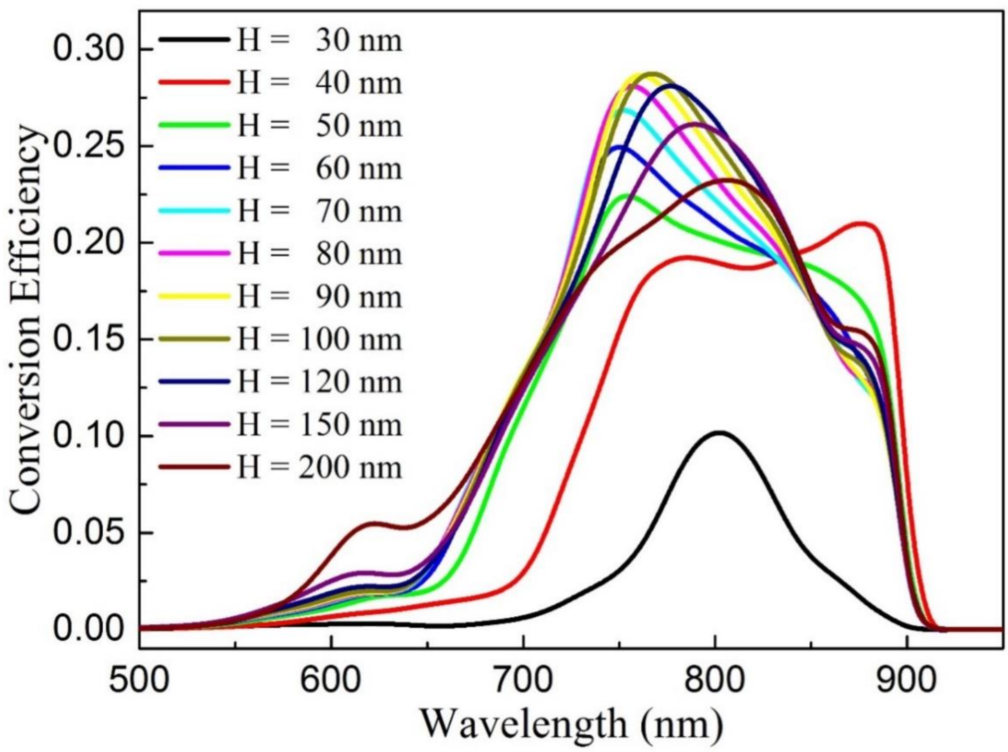

Fig. S10 Dependence of the conversion efficiency on the height of the HSQ pillars.